Hindawi Publishing Corporation
International Journal of Rotating Machinery
Volume 2007, Article ID 10940, 11 pages
doi:10.1155/2007/10940

Research Article

Numerical Simulation of the Transitional and Unsteady Flow through a Low Pressure Turbine

Romuald Skoda,[1] Rudolf Schilling,[1] and Meinhard T. Schobeiri[2]

[1] *Institute of Fluid Mechanics, Munich University of Technology, 85747 Garching, Germany*
[2] *Turbomachinery Performance and Flow Research Laboratory, Texas A&M University, College Station, TX 77843-3123, USA*

Received 9 March 2006; Revised 26 August 2006; Accepted 16 October 2006

Recommended by Shimpei Mizuki

A simulation strategy is developed for the computation of the time-accurate flow through low pressure turbines with periodically impinging wakes generated by moving cylinder rods. For the simulations, different time steps and turbulent inflow conditions and their impact on the laminar separation on the suction side are considered. A realizable cubic low-Reynolds number $k-\varepsilon$ turbulence model and a linear V2F model are utilized to capture transitional effects, in particular the laminar separation bubble at the suction side. For comparison with experimental data, published in a companion paper, pressure distribution and boundary layer profiles of the mean and fluctuation RMS velocity are considered. While the periodically disturbed flow is predicted with a reasonable accuracy by each model, for the undisturbed flow, an additional realizability condition based on a turbulent time scale bound is incorporated into the cubic model in order to capture the reattachment of the flow.

1. INTRODUCTION

The flow field in low pressure turbines is characterized by the laminar-turbulent transition and unsteady effects due to blade row interaction. Many recent experimental and numerical studies on the periodically disturbed flow in low pressure turbines are based on test facilities with circular cylinder rods to simulate the incoming wake. While there are first efforts to simulate the flow by a direct and large eddy simulation, see Wissink [1], Kalitzin et al. [2], and Fujiwara et al. [3], for technical problems, a statistical approach and the use of turbulence models are a more reasonable strategy.

When the Reynolds averaged Navier-Stokes equations (RANS) are considered for the simulation of transitional flows, the transition process is usually captured by transition models, consisting of a function determining the intermittency distribution and a criterion fixing the onset of the transition. Most models use boundary layer data, as the momentum loss thickness and the turbulence level at the boundary layer edge. Their numerical determination is difficult and based on the assumption of steady flow conditions.

Eddy viscosity turbulence models taking near-wall effects into account are, at least in principle, able to predict transition. The quality of the results is mainly determined by the near-wall treatment of the turbulence quantities. In the case of low-Reynolds number models, an empirical damping function is introduced to force the proper near-wall behavior of the eddy viscosity. Strictly, this damping function is only valid for the flow it has been calibrated for. Durbin [4] suggested the use of an additional transport equation for a velocity scale v^2, taking nonlocal effects into account by an elliptic operator f. Therefore, the $v^2 - f$ model (V2F) uses the more suitable velocity scale v^2 instead of the kinetic energy k in the eddy viscosity relation, and no damping functions are necessary to describe the correct near-wall behavior of the eddy-viscosity and of the ε-equation.

In many recent studies on wake induced transition, see for example Michelassi et al. [5] and Suzen and Huang [6], transition models are omitted and the "pure" turbulence model is applied to the laminar and transitional flow regions. While these authors use the $k-\omega$ model, that predicts a fully turbulent flow in any flow region, Skoda et al. [7] and Thermann et al. [8] obtained fairly good results with $k-\varepsilon$-based low-Reynolds number models and observed that the careful suppression of the stagnation point anomaly is critical for the success of a simulation. The stagnation point anomaly is not covered by the usual modification of the production term by Kato and Launder [9], since this approach can have

undesirable effects in flow regions not immediately influenced by the stagnation flow, but by a suitable realizability condition.

In a former investigation on a high pressure turbine cascade with a wake-generating cylinder row, see Skoda et al. [7], the authors found that the V2F model of Durbin [4], used in its "code-friendly" version of Lien et al. [10], was able to capture the wake-induced effects with a good accuracy, even without the use of a transition model. In particular, the onset and the end of transition were well captured by the model. The main aim of the present study is to investigate the performance of this and other models, that is, nonlinear low-Reynolds number $k-\varepsilon$ models, for the flow through a low pressure turbine, which is much more complicated due to the laminar separation with turbulent reattachment. The computational results are compared with experimental data, which are documented in detail in a companion paper by Schobeiri and Öztürk [11].

2. NUMERICAL APPROACH

For all simulations presented, the two-dimensional, parallel solver NS2D developed by the authors is used. NS2D is a colocated, cell-centred, and block-structured finite volume method using the SIMPLE scheme for pressure-velocity coupling. For the interpolation of the mass fluxes at the cell faces, Rhie and Chow's method is used. At the block interfaces, the grid lines do not need to match, while the accuracy of the discretization scheme is maintained by a locally unstructured treatment of the fluxes. This means that a cell adjacent to an interface may have an arbitrary number of faces. This approach is also utilized for sliding interfaces. The convective terms of all equations are approximated using the second-order SMART scheme by Gaskell and Lau [14] in combination with a deferred correction approach. The implicit three-level time discretization is of second-order accuracy. The parallelization of the code is based on MPI-libraries (message passing interface), and the sets of linear equations are solved using the strongly implicit procedure by Stone [15].

For turbulence modelling, two classes of eddy viscosity models are used, namely, the cubic low-Reynolds number $k-\varepsilon$ model of Lien et al. [12] (LCL) and the v^2-f model of Durbin [4] (V2F). The LCL model is able to take into account Reynolds-stress anisotropy effects by a cubic constitutive relation between the Reynolds-stress tensor and the mean flow quantities. The authors of the LCL model propose a realizability constraint, where C_μ in the eddy viscosity relation is expressed as a function of the strain and rotation invariants S and Ω.

In NS2D, the "code-friendly" implementation of the V2F model, see Lien et al. [10], is based on the following equations for the velocity scale v^2 and the elliptic operator f:

$$\frac{\partial v^2}{\partial t}+u_j\frac{\partial v^2}{\partial x_j}=kf-6v^2\frac{\varepsilon}{k}+\frac{\partial}{\partial x_i}\left[\left(\upsilon+\frac{\upsilon_t}{\upsilon_k}\right)\frac{\partial v^2}{\partial x_i}\right],$$

$$L^2\frac{\partial^2 f}{\partial x_j^2}-f=\frac{1}{T}\left[(D_1-6)\frac{v^2}{k}-\frac{2}{3}(D_1-1)\right]-D_2\frac{P_k}{k}. \tag{1}$$

The time and length scales T and L are calculated with the realizability condition of Durbin [13]:

$$T=\min\left[\frac{k}{\sqrt{6}C_\mu u_t^2\sqrt{S_{ij}S_{ij}}}\right], \tag{2}$$

$$L=C_L\min\left(\frac{k^{1.5}}{\varepsilon},\frac{1}{\sqrt{6}}\frac{k^{1.5}}{C_\mu u_t^2\sqrt{S_{ij}S_{ij}}}\right). \tag{3}$$

No additional modification of the production term to suppress the stagnation point anomaly is applied. The Reynolds-stress tensor is calculated via the Boussinesq-Ansatz. The constants specific to the V2F model are $D_1=1.4$, $D_2=0.3$, $C_L=0.17$. In the ε-equation, the constants are $C_{\varepsilon 2}=1.92$ and the constant $C_{\varepsilon 1}=1.55+\exp(-0.00285\cdot \mathrm{Re}_y^2)$ is a function of the turbulent Reynolds number $\mathrm{Re}_y=\sqrt{k}/y\upsilon$, where y is the wall distance. The eddy viscosity is calculated by $\upsilon_t=C_\mu v^2 T$ with $C_\mu=0.19$. The turbulent velocity scale in (2) and (3) is $u_t^2=v^2$. The time and length scales are bounded from below by the corresponding Kolmogorov scales, see Durbin [4].

In order to incorporate a more effective realizability condition in the LCL model, a bound of the time scale is incorporated according to (2), where $u_t^2=f_\mu\cdot k$. This variant of the model is referred to as LCL-RD, and the eddy viscosity relation in the LCL-RD model can be written as

$$\upsilon_t=\frac{2/3}{4+S+0.9\cdot\Omega}\cdot f_\mu\cdot k\cdot T. \tag{4}$$

The ε-equation is implemented in explicit dependence on the turbulent time scale T in order to adopt realizability:

$$\frac{\partial\varepsilon}{\partial t}+u_j\frac{\partial\varepsilon}{\partial x_j}=\frac{C_{\varepsilon 1}\cdot P_k-C_{\varepsilon 2}\cdot\varepsilon}{T}+\frac{\partial}{\partial x_i}\left[\left(\upsilon+\frac{\upsilon_t}{\sigma_\varepsilon}\right)\frac{\partial\varepsilon}{\partial x_i}\right]. \tag{5}$$

The convergence criterion for each equation in any model is a decrease of the sum norm of the residuum of at least 6 orders of magnitude. For any test case considered, at the inlet, the velocity field and the turbulence values k and ε are prescribed, v^2 equals $2/3k$, and f is extrapolated. At the outlet, a constant value of the static pressure is specified.

3. VALIDATION

The success of the simulation of the low pressure turbine flow is considered to be dominated by two main influences: firstly, the laminar separation at the suction side is accompanied by an upstream located stagnation point flow that can cause a stagnation point anomaly. Secondly, the unsteady effects are to be taken into account by sufficiently fine temporal resolution. Therefore, the first issue is isolated by the flow over a flat plate with a semicircular leading edge, the ERCOFTAC test case T3L, and the second one is considered by a systematic time-step refinement on the cylinder flow, where the highest frequencies in the flow field occur.

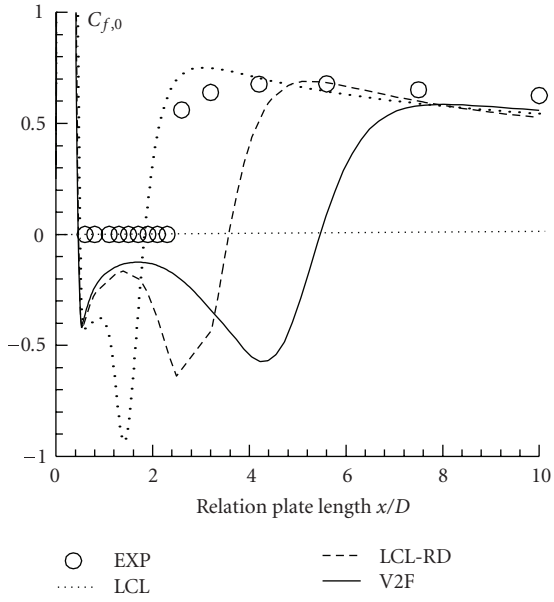

FIGURE 1: T3L$_3$: wall shear stress.

3.1. Flat plate with semicircular leading edge

The ERCOFTAC test case T3L$_3$, a flat plate with a semicircular leading edge with diameter D, an inlet turbulence intensity of Tu = 2.3%, and a free stream velocity of $u_{\text{in}} = 5.0$ m/s, are investigated. The spatial resolution is the same as in the investigation of Thermann et al. [8], so that the results are assumed to be grid-independent. Downstream of the leading edge, a laminar separation with a turbulent reattachment occurs. Thermann et al. [8] utilize another version of the V2F model by Lien et al. [10], which deviates from the present one in the formulation of $C_{\varepsilon 1}$ that does not explicitly depend on the wall distance. However, the wall-distance free V2F model predicted a much too low production of turbulence in the laminar separation bubble and is therefore substituted by the version described in the previous section. In Figure 1, the wall shear stress $C_{f,0}$ is shown, which is defined as

$$C_{f,0} = \frac{\tau_w}{(\rho/2)u_{\text{in}}^2}. \tag{6}$$

While the LCL model predicts the reattachment point too early compared with the experiment, where it was located at $x/D = 2.2$, the LCL-RD model overestimates the length of the laminar separation bubble slightly. The present version of the V2F model still predicts the reattachment too far downstream, at $x/D \approx 5$. However, this is still an improvement compared to the results obtained by Thermann et al. [8], where the wall-distance free V2F version determines the reattachment point to be located at $x/D = 9$. Figure 2 shows contours of the turbulence intensity Tu. To allow comparison with the single hot-wire measurements, simulation results were evaluated by

$$\text{Tu} = \frac{\sqrt{2k/3}}{u_{\text{in}}}, \tag{7}$$

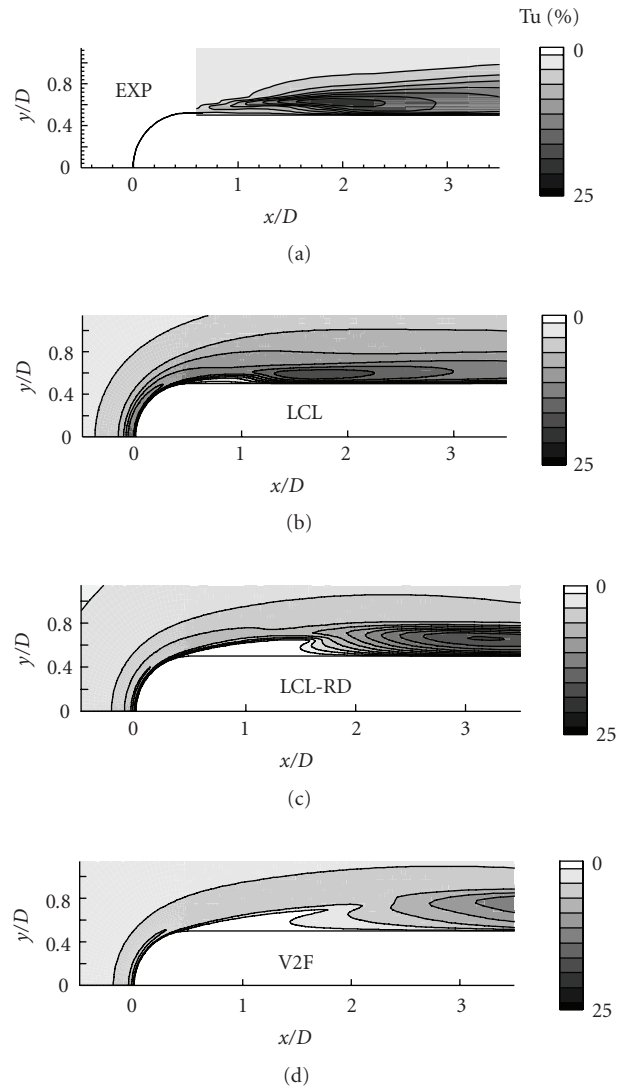

FIGURE 2: T3L$_3$: turbulence intensity.

assuming isotropic turbulence. The V2F model calculates a too low level of turbulence in the shear layer between the separation bubble and the mean flow, resulting in a too long bubble. Calculations with switched off realizability bound (these results are not presented here) show still a too low turbulence production and a too long bubble. This is caused by the production term formulation including v^2. Both the LCL and LCL-RD models determine a higher level of turbulence in the shear layer, and the LCL model yields the most reasonable agreement of the bubble size with the experimental data. However, since there are regions of high turbulence intensity at the leading edge of the plate, see Figure 2(b), the LCL model does not completely suppress the stagnation point anomaly. This turbulent flow region is convected downstream, leading to highly turbulent regions around and within the laminar separation bubble. This stagnation point anomaly is much less distinctive with the LCL-RD and the V2F models.

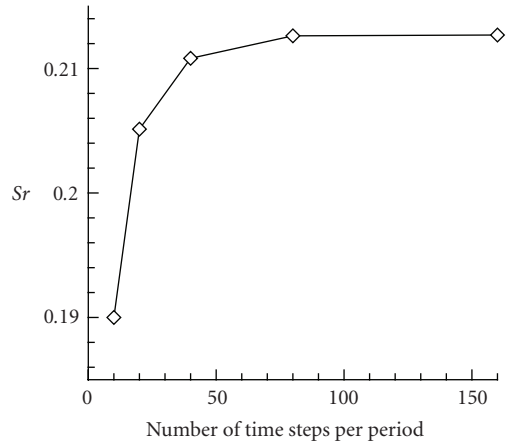

Figure 3: Strouhal number in dependence on the temporal resolution.

3.2. Vortex shedding behind a circular cylinder

Taking unsteady flow features into account, results for the vortex shedding of a free standing circular cylinder at $\mathrm{Re}_D = 900$, corresponding to the wake generating row of cylinders in front of the turbine blade cascade, are considered. Special attention is paid to the temporal convergence characteristics of the test case. For the LCL model, a varying time step is used while the spatial resolution remains fixed. The same O-grid with 320×80 cells as for the cylinder-blade interaction investigation is used and a local y^+ value of the wall-adjacent cells lower than 0.1 is guaranteed. In Figure 3, the Strouhal number Sr depending on the time step is shown, displaying that a temporal resolution of 80 time steps per period yields a time-step independent solution.

4. LOW PRESSURE TURBINE

In the following, details of the numerical model for the simulation of the low pressure turbine flow, without and with cylindrical rods, are presented. Firstly, a brief overview of the experimental setup is given, which is described in detail by the companion paper of Schobeiri and Öztürk [11].

4.1. Experimental investigation

For the low pressure turbine cascade, consisting of 5 blades, time-averaged pressure measurements and single hot-wire results at the suction side are available for both, the undisturbed and periodically disturbed cases. For the latter, the measured velocities are phase-averaged. The pressure is recorded at a Reynolds number of $\mathrm{Re}_C = 110\,000$, while the mean velocities and the turbulence level are measured at $\mathrm{Re}_C = 100\,000$ and $\mathrm{Re}_C = 125\,000$. In Figure 4, the hot wire traverses are shown. On the pressure side, no boundary layer information, but the fact that a small laminar separation bubble is present, is available. All measurements were done in a low-speed wind channel, so that incompressible flow conditions can be assumed.

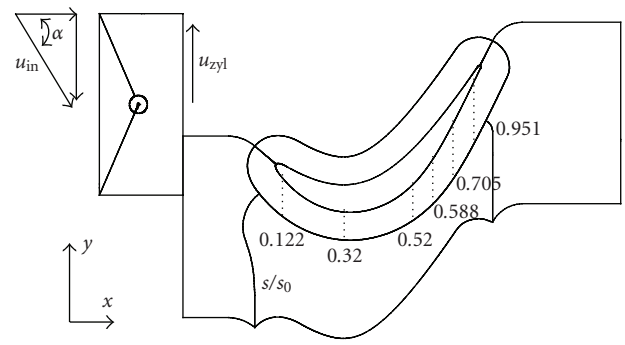

Figure 4: Computational domain and measurement positions.

Table 1: Geometry and operation parameters.

Inlet velocity	$u_{in} = 4$ m/s
Rod translational speed	$u_{cyl} = 5$ m/s
Inlet angle	$\alpha = 30^\circ$
Rod diameter	$D_{cyl} = 2$ mm
Rod spacing	$S_{cyl} = 163$ mm
Inlet turbulence intensity	Tu = 1.0%
Blade Reynolds number	Re = 110 000
Blade pitch	$S_B = 163$ mm

4.2. Numerical model

Figure 4 shows the 2D computational domain with the wake inducing cylinder rods. In Table 1, the main geometry and operation parameters are documented. The total number of nodes is about 100 000, and a nondimensional wall distance $y^+ < 0.1$ is guaranteed at any wall. According to the experiences of the authors, see Skoda et al. [7] and Thermann et al. [8], this spatial resolution is sufficiently fine. The pitch of the cylinder rod S_{cyl} is, compared to the experimental setup, slightly adjusted in order to equal the blade pitch S_B. At the sliding interface, the nonmatching treatment described in Section 2 is utilized, so that the accuracy of the conservative scheme is maintained.

Despite the fact that the geometrical inlet angle equals $\alpha = 35^\circ$ in the experiment, velocity measurements very close to the leading edge indicated that the average flow angle is $\alpha = 30^\circ$. Preliminary calculations have shown that a variation of α in this range does hardly effect the separation on the suction side, but has a significant influence on the pressure distribution on the blade.

Regarding the turbulent inflow conditions, the kinetic energy k_0 is fixed by the measured turbulence level Tu = 1.0% and the inflow velocity u_{in}. For the determination of the dissipation rate ε, a turbulent length scale is assumed to be $L = 0.07 \cdot H$, where the height of the test section is $H = 5 \cdot S_B$. The dissipation rate ε_0 at the inlet is assumed to equal

$$\varepsilon_0 = C_\mu^{3/4} \cdot \frac{k^{1.5}}{L}. \tag{8}$$

To quantify the used time-step size DT, the cylinder passing time T, which is given below, is utilized for referencing any time scale.

4.3. Undisturbed inflow conditions

Despite the fact that the flow is not disturbed, vortex shedding occurs at the trailing edge of the blade and makes a steady solution difficult. Only for the LCL-RD model, a higher order steady state solution could be obtained. For the LCL and the V2F models, two different time steps, corresponding to $DT_1 = 0.72 \cdot T$ and $DT_2 = 0.0034 \cdot T$, are investigated.

In the following, the influence of the inlet value of ε and of the time-step size is evaluated by the pressure and wall shear stress distribution on the blade as well as by velocity and turbulence profiles on the suction side. Afterwards, results obtained with different turbulence models are compared.

4.3.1. Influence of the inflow condition of ε

Addressing the influence of the inlet boundary condition for ε, for DT_1 the value of ε_0 is varied by one order of magnitude, see Figure 5, resulting in $\varepsilon_1 = 10 \cdot \varepsilon_0$ and $\varepsilon_{-1} = 0.1 \cdot \varepsilon_0$. For comparison of the different inflow values of ε, the LCL model is applied. Regarding the pressure distribution, see Figure 5(a), the experimental data of both adjacent Reynolds numbers, $\mathrm{Re}_C = 100\,000$ and $\mathrm{Re}_C = 125\,000$, are included for reference. The pressure coefficient is defined as follows:

$$C_p = \frac{p_w}{(\rho/2)u_{\mathrm{in}}^2}. \tag{9}$$

None of the inflow conditions result in an acceptably good prediction of the pressure distribution. A variation of the inflow angle does influence but not improve the results, so that probably secondary flow effects are present in the experiment. In Figure 5(b), the wall shear stress coefficient, which is defined in (6), at the suction side is shown. In addition to the shear stress from the simulations, the experimentally determined separation (S) and reattachment (R) points on the suction side are included. According to the experiment, the flow separates at $s/s_0 = 0.55$ and reattaches at $s/s_0 = 0.746$. For the case ε_{-1}, the flow remains attached, while for the other two values of ε, the measured separation is well captured. However, the reattachment is not predicted.

A more detailed insight is provided by the mean velocity and turbulence level profiles on the suction side that are plotted over the y-coordinate, see Figure 6. The reference length is $y_{\mathrm{ref}} = 10$ mm. Figure 5 suggests a suitable dissipation value $\varepsilon_{-1} < \varepsilon < \varepsilon_0$. This is confirmed by the velocity plots in Figure 6(a). However, Figure 6(b) shows that for both, ε_{-1} and ε_0, the free stream turbulence is too high and therefore ε is too low. On the other hand, the LCL model does not suppress the stagnation point anomaly sufficiently, resulting in turbulent flow regions at the leading edge which are convected downstream. This fact will be evident with the V2F model, which is discussed in the next section. Both effects, too low inlet value of ε and stagnation point anomaly, are counteracting. For all simulations shown in the following sections, the case ε_0 is chosen.

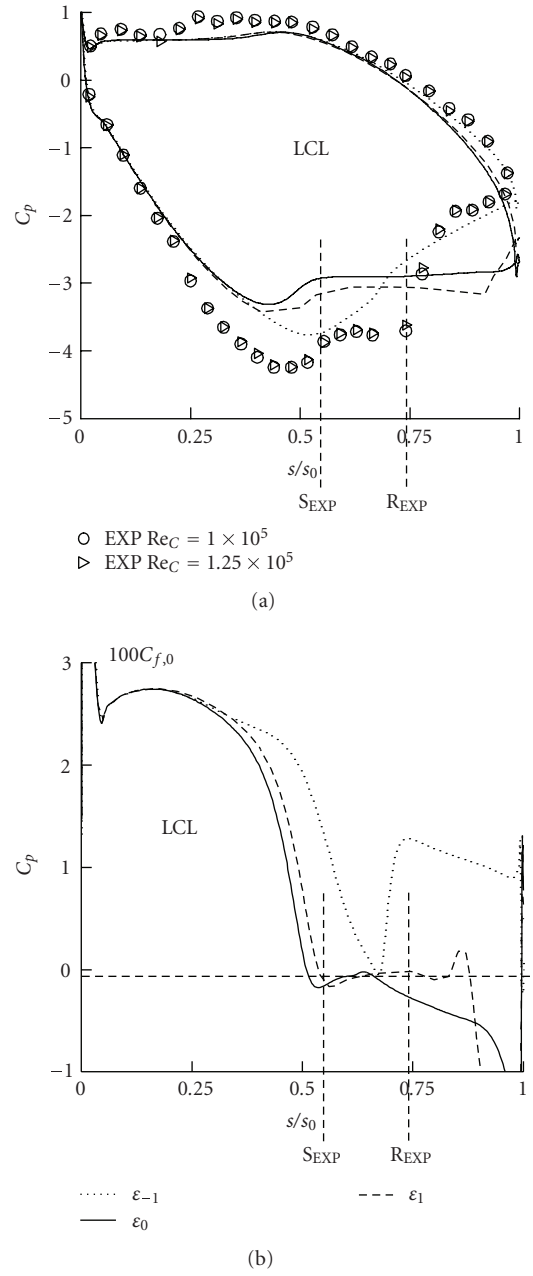

Figure 5: Pressure coefficient and wall shear stress coefficient on the suction side for different inlet values of ε for the undisturbed flow.

4.3.2. Influence of the time step

Regarding the time step, in Figure 7(a) the wall pressure is shown for both time steps for the LCL and V2F turbulence models. It is obvious that the time-step size has almost no influence when used with the LCL model and only a small impact with the V2F model on the pressure distribution. For the

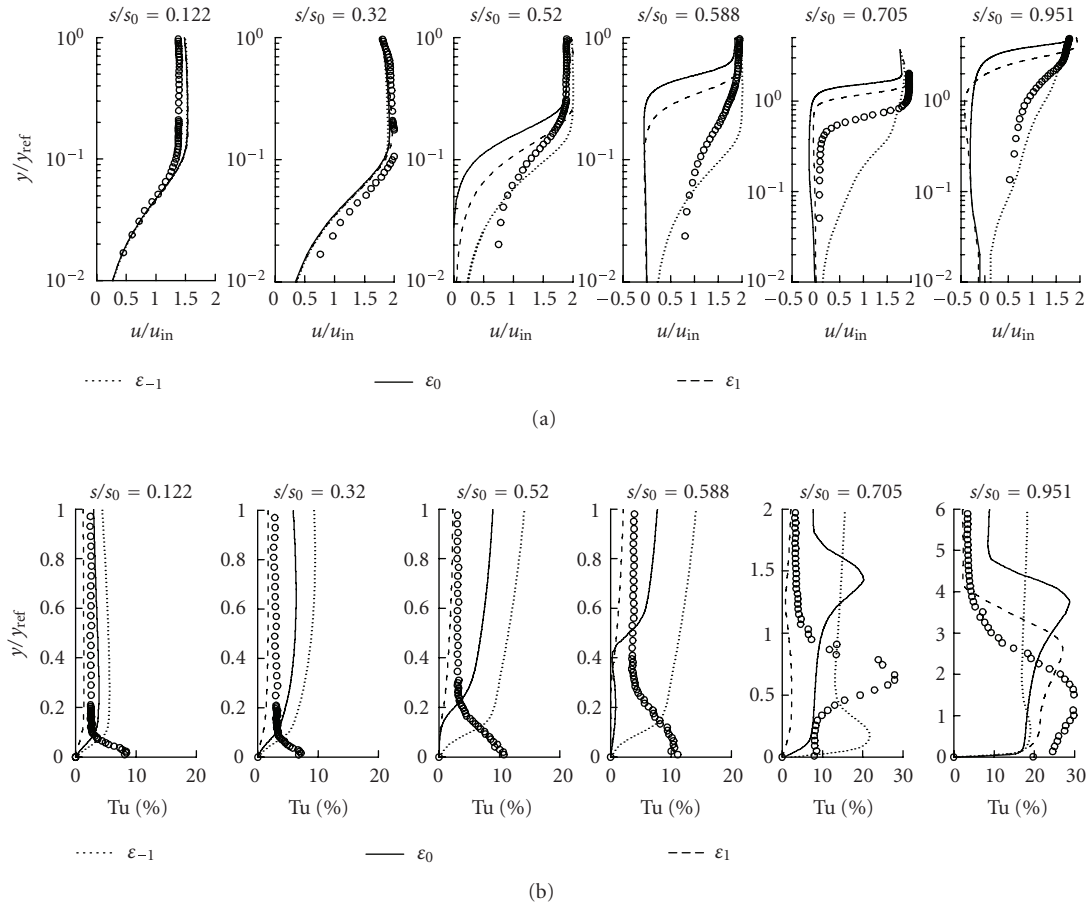

Figure 6: Velocity and turbulence profiles on the suction side for different inlet values of ε for the undisturbed case with the LCL model.

LCL-RD model, the steady state result is shown in Figure 7. In the following sections, where available, results obtained with time-step DT_2 are discussed.

4.3.3. Influence of the turbulence model

While the agreement between experiment and simulation is relatively good for the LCL-RD model, the pressure on the suction side is far too high for the LCL and V2F models, see Figure 7(a). The better performance of the LCL-RD model is also reflected in the wall shear stress distribution on the pressure side (PS) and on the suction side (SS), see Figure 7(b). The suction side separation is relatively well captured by any model, best by the V2F model. However, only the LCL-RD model predicts the reattachment of the flow, while the others determine a separated flow down to the trailing edge. This fact is also distinctive in the pressure distribution, see Figure 7(a).

Regarding the velocity and turbulence intensity profiles on the suction side, see Figure 8, the LCL-RD model predicts the velocity profiles with a higher accuracy than the other models. Since the LCL and V2F models do not capture the reattachment, which is evident from the experimental data, the simulated velocity profiles deviate significantly from the measured ones for these models. Focusing on the turbulence level profiles, it becomes clear that the LCL and the V2F models predict a delayed transition and an essentially laminar boundary layer at the separation point. The LCL-RD model shows a local maximum of the turbulence intensity close to the wall at $s/s_0 = 0.52$, indicating the laminar-turbulent transition process. It could be expected that the V2F model shows a better behavior in transitional flow, in particular captures the stress anisotropy responsible for the transition process, see Thermann et al. [8]. However, here, it predicts an almost laminar boundary layer, and the LCL-RD model seems to be superior to the V2F model.

For a position immediately behind the separation, for the LCL-RD model, the laminar separation bubble can be discerned at $s/s_0 = 0.588$ with a very low turbulence intensity inside the bubble. This observation, which is not distinctive in the experiment, is consistent with the results on the validation test case T3L. For the LCL and V2F models, the same statement is valid, while the lateral extent of the laminar separation bubble is much bigger than for the LCL-RD model. The additional realizability constraint in the LCL-RD model does not suppress the stagnation point anomaly sufficiently, which is evident by the free stream turbulence level in Figure 8(b).

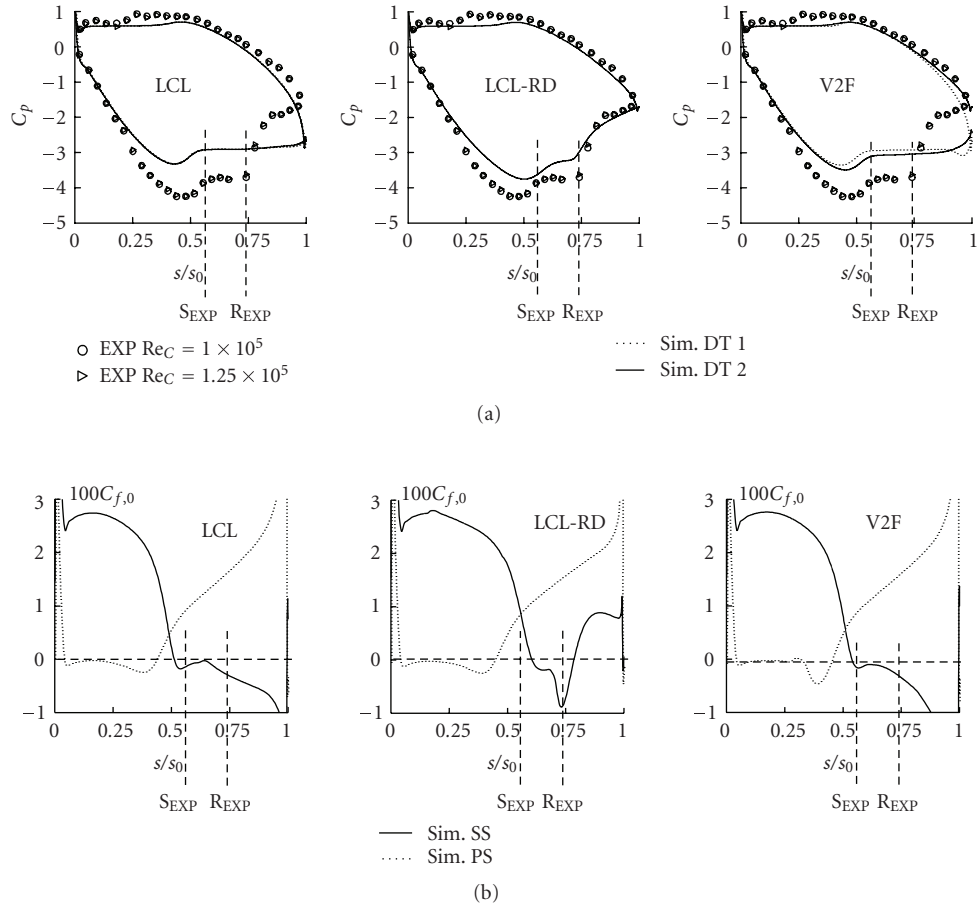

Figure 7: Pressure coefficient and wall shear stress coefficient for different turbulence models for the undisturbed flow.

4.4. Periodically disturbed inflow conditions

The chosen time step corresponds to the validation on the circular cylinder flow. Thus, a time step corresponding to 80 time steps per cylinder wake period is used, resulting in a very fine temporal resolution of $DT = 4.9 \cdot 10^{-4} \cdot T$, and more than 2000 time steps are used per cylinder rod passing time T. Therefore, it is ensured that even the high frequency cylinder vortex shedding is resolved in a time-step independent way. Before the results are averaged over one cylinder passing period T, at least 4 cylinder passages are calculated to ensure that no influences from the initial solution are present. Figure 9 shows for the LCL model the drag and lift coefficients C_x and C_y, in the x- and y-directions, respectively, according to Figure 4. These coefficients are defined as the sum of the pressure and wall shear stress coefficients in the respective direction. The presence of the high-frequency cylinder vortex shedding is obvious.

Addressing the pressure distribution, see Figure 10(a), a good agreement with the experimental data can be found for each model. In particular, the reattachment of the flow is captured. According to the experiment, the separation S occurs at the same location as for the undisturbed flow, while for the periodically disturbed flows, the reattachment R takes place further upstream at $s/s_0 = 0.664$, and therefore the separation bubble decreases in size. The computed wall shear stress distribution is plotted in Figure 10(b) and indicates that on the suction side, the separation point is predicted too far downstream and the bubble length is overestimated by each turbulence model, in particular by the V2F model.

The measured velocity profiles on the suction side, see Figure 11(a), are barely influenced by the impinging wakes and are almost the same as for the undisturbed case. Due to the captured reattachment of the flow by each turbulence model, the agreement between the experiment and the simulation is much better than for the undisturbed case.

The profiles of the turbulence intensity, see Figure 11(b), show that, according to the experiment, the time-averaged effect of the wake impingement can mainly be identified as an increase of the free stream level of turbulence. While this fact is properly captured by the LCL and LCL-RD models, the V2F model determines a free stream turbulence intensity level that is essentially the same as that for the undisturbed case. The LCL-RD and the V2F models predict the presence of the local maximum of turbulence generated by the shear layer between the laminar separation and the free stream quite well. The V2F model performs slightly better than the LCL-RD model. For the LCL model, the turbulence

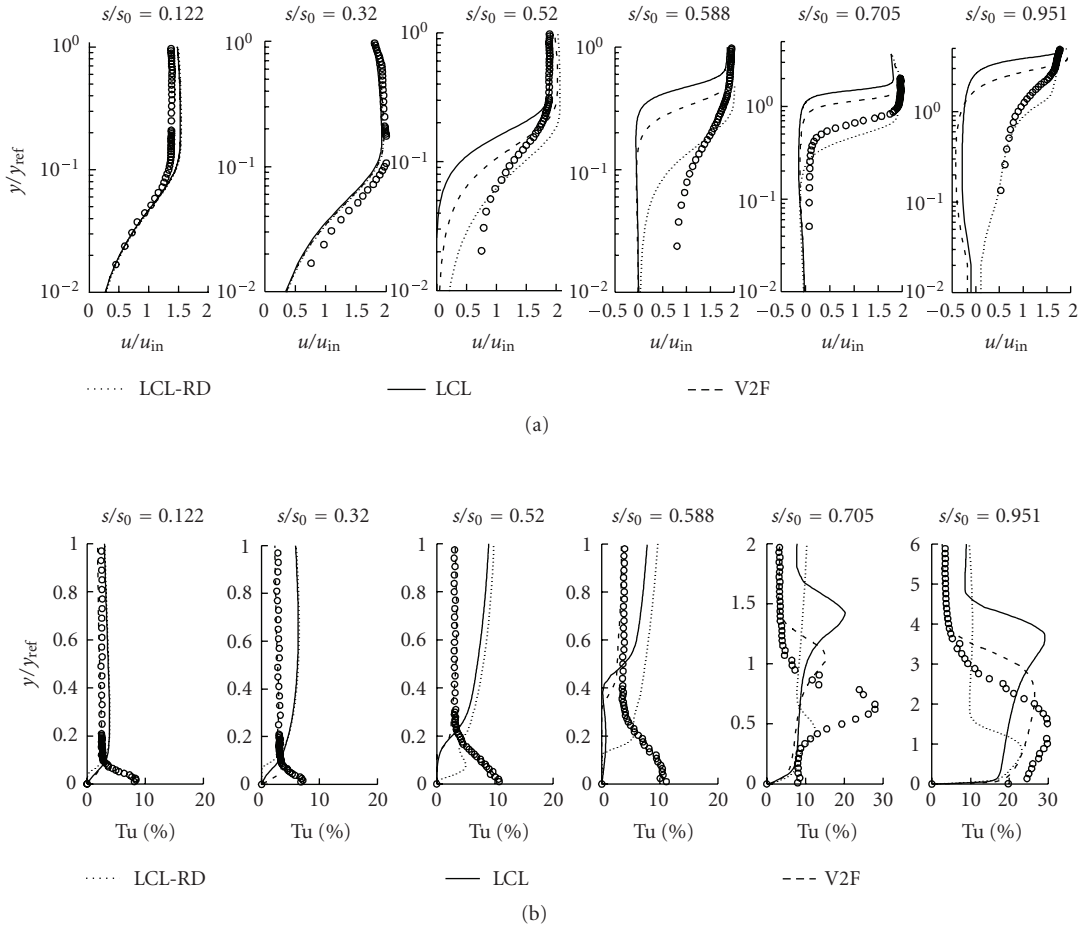

Figure 8: Velocity and turbulence profiles on the suction side for different turbulence models for the undisturbed case.

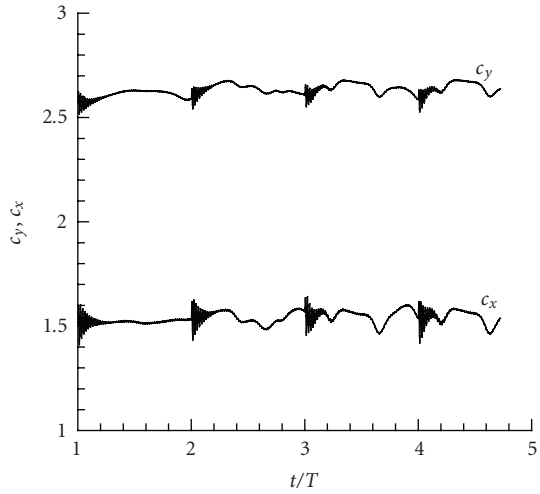

Figure 9: Lift and drag coefficients for the LCL model for the periodically disturbed flow.

profile in and downstream of the separation is even qualitatively wrong.

5. CONCLUSIONS

A numerical simulation of the undisturbed and periodically disturbed flow on a low pressure turbine cascade has been performed. The periodic disturbances have been modeled in a way that the wake generating cylinder rods have been included into the computational domain and their movement has been taken into account for the time-accurate simulations. A comprehensive study on the performance of the models in laminar separating flow, on the temporal resolution, and on the turbulent inlet boundary conditions has been performed. While for the undisturbed flow, only the modified LCL model captures the reattachment of the suction side flow, for periodically disturbed flow conditions, all models show a reasonable performance. Regarding the turbulence profiles on the suction side, the realizable LCL-RD model is superior over the original LCL model, whereas the superiority of the V2F model, which has been observed in former investigations, could not be confirmed here.

Further investigations on unsteady test cases need to be done to highlight the features of these turbulence models regarding separation, transition, stagnating flow, and influence of the temporal discretization. It is crucial that the inflow conditions are experimentally determined in more detail. In

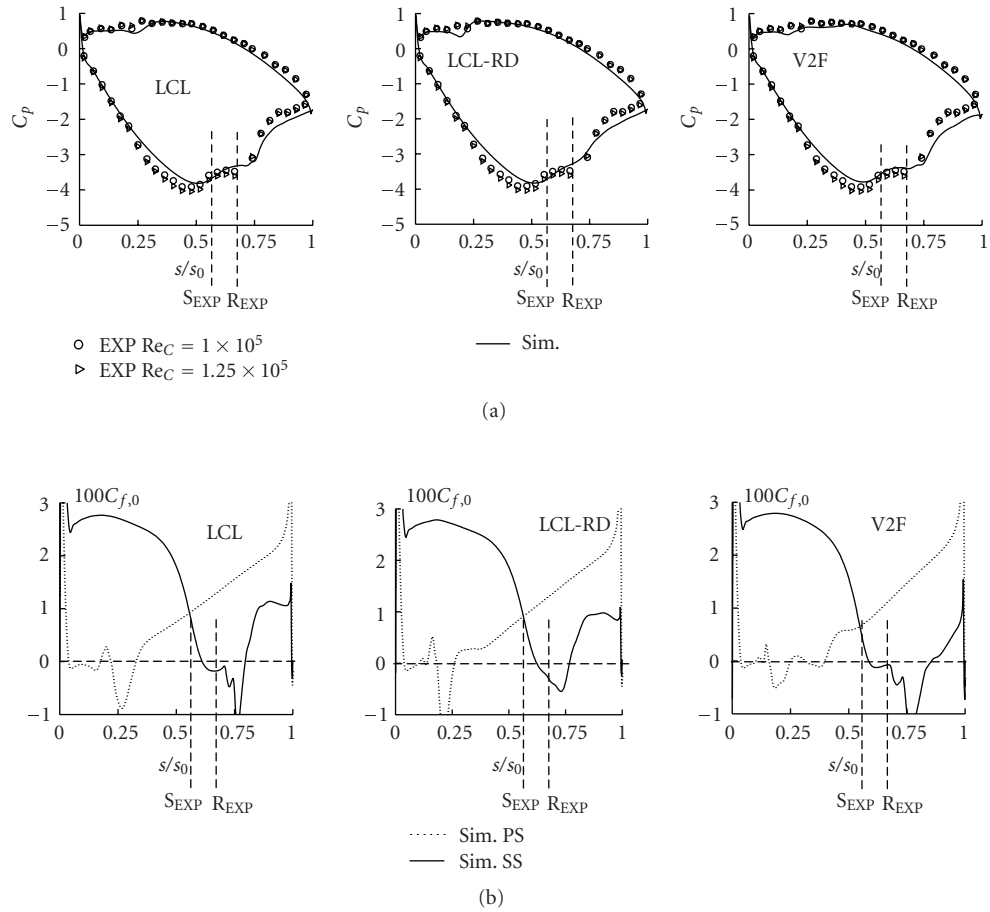

Figure 10: Pressure coefficient and wall shear stress coefficient for different turbulence models for the periodically disturbed case.

particular, it is necessary to know the integral time and length scales of turbulence in the inflow in order to make a reliable estimation of the turbulence decay and to specify proper turbulent inflow conditions for the simulation. Then, the performance of the V2F model, which is unsatisfactory in the present investigation, will be enlightened in more detail with unsteady data.

NOMENCLATURE

Symbols

$C_L, C_\mu, C_{\varepsilon 1}, C_{\varepsilon 2}$:	Turbulence model constants
$C_{f,0}$:	Shear stress coefficient
C_p:	Pressure coefficient
D:	Diameter
D_1, D_2:	Turbulence model constants
DT:	Time step
f:	Elliptic operator
f_μ:	Damping function
H:	Test section height
k:	turbulent kinetic energy
p:	Pressure
P_k:	Turbulent production
L:	Turbulent length scale
Re:	Reynolds number
S_{ij}:	Strain rate tensor
S:	Invariant of the strain rate tensor; spacing
Sr	Strouhal number
t:	Time
T:	Turbulent time scale; cylinder passing time
Tu:	Turbulence intensity
u:	Velocity
u_t:	Turbulent velocity scale
v^2:	Turbulent velocity scale in the V2F model
x, y:	Spatial coordinates
α:	Flow angle
ε:	Turbulent dissipation rate
ρ:	Density
τ:	Shear stress
υ, υ_t:	Laminar and turbulent viscosities
Ω:	Invariant of the rotation tensor

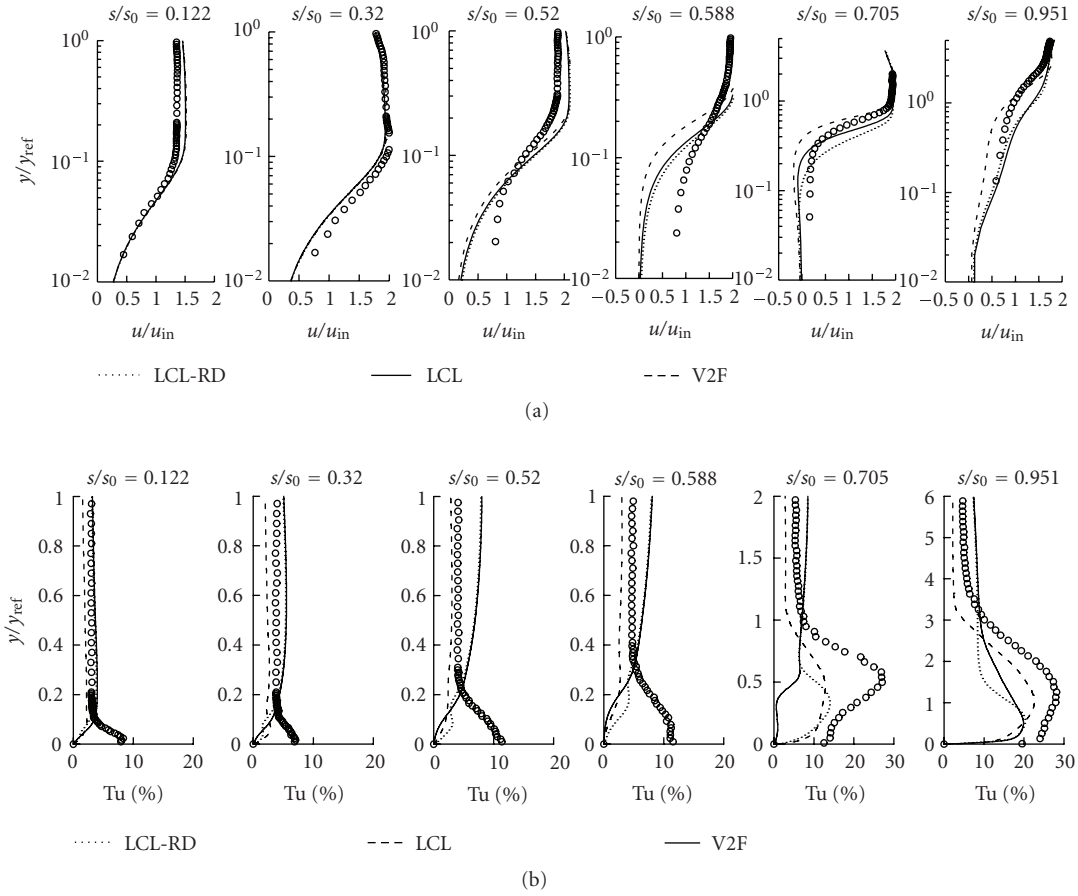

Figure 11: Velocity and turbulence profiles on the suction side for the periodically disturbed case.

Subscripts

0, ref:	Reference
B:	Blade
C:	Blade chord
EXP:	Experiment
i, *j*:	Coordinate indexes
in:	Inlet
cyl:	Cylinder
w:	Wall

Abbreviations

ERCOFTAC:	European Research Community on Fluids Turbulence and Combustion
EXP:	Experiment
LCL:	Model of Lien et al. [12]
LCL-RD:	Model of Lien et al. [12] with realizability of Durbin [13]
PS:	Pressure side
S:	Separation
SS:	Suction side
R:	Reattachment
RANS:	Reynolds-averaged Navier-Stokes equations
RMS:	Root mean square
V2F:	$v^2 - f$-model

ACKNOWLEDGMENT

Romuald Skoda and Rudolf Schilling wish to appreciate the financial support by the Federal Ministry of Economies and Technology (BMWI) in the framework of the "Zukunfts-Innovations-Programm (ZIP)," code 0327294C.

REFERENCES

[1] J. G. Wissink, "DNS of separating, low Reynolds number flow in a turbine cascade with incoming wakes," in *Proceedings of the 5th International Symposium on Engineering Turbulence Modelling and Experiments*, W. Rodi and N. Fueyo, Eds., pp. 731–740, Mallorca, Spain, September 2002.

[2] G. Kalitzin, X. Wu, and P. A. Durbin, "DNS of fully turbulent flow in a LPT passage," in *Proceedings of the 5th International Symposium on Engineering Turbulence Modelling and Experiments*, W. Rodi and N. Fueyo, Eds., pp. 741–750, Mallorca, Spain, September 2002.

[3] H. Fujiwara, P. R. Voke, and C. Arakawa, "Large-eddy simulation of TL10 LP turbine blade row," in *Proceedings of the 5th International Symposium on Engineering Turbulence Modelling and Experiments*, W. Rodi and N. Fueyo, Eds., pp. 751–758, Mallorca, Spain, September 2002.

[4] P. A. Durbin, "Separated flow computations with the k-ε-v^2 model," *AIAA Journal*, vol. 33, no. 4, pp. 659–664, 1995.

[5] V. Michelassi, J. G. Wissing, and W. Rodi, "DNS, LES and URANS of periodic undteady flow in a LP turbine cascade: a comparison," in *Proceedings of 5th European Conference on Turbomachinery*, pp. 1185–1195, Prague, Czech Republic, March 2003.

[6] Y. B. Suzen and P. G. Huang, "Numerical simulation of wake passing on turbine cascades," in *Proceedings of the 41st AIAA Aerospace Science Meeting & Exhibition*, Reno, Nev, USA, January 2003, AIAA paper 2003-1256.

[7] R. Skoda, R. Schilling, J. Thurso, and B. Stoffel, "Numerical simulation of unsteady and transitional flows pertaining to turbine cascades," in *Proceedings of the 5th International Symposium on Engineering Turbulence Modelling and Experiments*, W. Rodi and N. Fueyo, Eds., pp. 759–768, Mallorca, Spain, September 2002.

[8] H. Thermann, M. Müller, R. Niehuis, R. Skoda, and R. Schilling, "Numerical simulation of the flow in an annular compressor cascade with different turbulence and transition models," in *Proceedings of the 5th European Conference on Turbomachinery*, pp. 937–946, Prague, Czech Republic, March 2003.

[9] M. Kato and B. E. Launder, "The modeling of turbulent flow around stationary and vibrating square cylinders," in *Proceedings of 9th Symposium on Turbulent Shear Flows*, pp. 1–6, Kyoto, Japan, August 1993.

[10] F. S. Lien, G. Kalitzin, and P. A. Durbin, "RANS modeling for compressible and transitional flows," in *Proceedings of Summer Programme*, CTR, Stanford University, Palo Alto, Calif, USA, 1998.

[11] M. T. Schobeiri and B. Öztürk, "Boundary layer separation on low pressure turbine blades under unsteady flow conditions," in *Proceedings of the 10th International Symposium on Transport Phenomena and Dynamics of Rotating Machinery (ISROMAC-10 '04)*, Honolulu, Hawaii, USA, March 2004, paper ISROMAC10-2004-124, submitted to *International Journal of Rotating Machinery*.

[12] F. S. Lien, W. L. Chen, and M. A. Leschziner, "Low- Reynolds-number eddy-viscosity modelling based on non-linear stress-strain/vorticity relations," in *Proceedings of the 3rd International Symposium on Engineering Turbulence Modelling and Experiments*, W. Rodi and E. Bergeles, Eds., pp. 91–100, Crete, Greece, May 1996.

[13] P. A. Durbin, "On the k-ε stagnation point anomaly," *International Journal of Heat and Fluid Flow*, vol. 17, no. 1, pp. 89–90, 1996.

[14] P. H. Gaskell and A. K. C. Lau, "Curvature-compensated convective transport: SMART, a new boundedness- preserving transport algorithm," *International Journal for Numerical Methods in Fluids*, vol. 8, no. 6, pp. 617–641, 1988.

[15] H. L. Stone, "Iterative solution of implicit approximations of multidimensional partial differential equations," *SIAM Journal on Numerical Analysis*, vol. 5, no. 3, pp. 530–558, 1968.